# Microstructure and dislocation structure evolution during creep life of Ni-based single crystal superalloys

Yu, Hao; Xu, Wei; van der Zwaag, Sybrand

**DOI**
10.1016/j.jmst.2019.11.028

**Publication date**
2020

**Document Version**
Final published version

**Published in**
Journal of Materials Science and Technology

Journal of Materials Science & Technology 45 (2020) 207–214

Contents lists available at ScienceDirect

Journal of Materials Science & Technology

journal homepage: www.jmst.org

Research Article

# Microstructure and dislocation structure evolution during creep life of Ni-based single crystal superalloys

Hao Yu[a], Wei Xu[a,b,*], Sybrand van der Zwaag[a]

[a] Novel Aerospace Materials Group, Faculty of Aerospace Engineering, Delft University of Technology, 2629HS, Delft, the Netherlands
[b] State Key Laboratory of Rolling and Automation, Northeastern University, 110819, Shenyang, China

ARTICLE INFO

*Article history:*
Received 27 September 2019
Received in revised form 7 November 2019
Accepted 7 November 2019
Available online 17 January 2020

*Keywords:*
Ni superalloys
Microstructure evolution
Dislocation behaviour

ABSTRACT

The high performance of Ni single crystal superalloys during high temperature low stress creep service, is intrinsically determined by the combined effects of microstructural evolution and the dislocation behaviour. In the field of the evolution of dislocation network, two main recovery mechanism based on dislocation migration dominate the process. One is superdislocations shearing into γ' rafts through a two-superpartials-assisted approach. Another is the compact dislocations migrating along γ/γ′ interface. These two mechanisms are similarly climb-rate-controlled process. In this work, a model for the minimum creep rate based on thermodynamic and kinetic calculations and using an existing detailed dislocation dynamics model has been built by taking the dislocation migration behaviours as well as the rafted microstructure into consideration, which can well reproduce the ([100] tensile) creep properties of existing Ni superalloy grades, without the need to make the dislocation parameter values composition dependent.



## 1. Introduction

Ni-based single crystal superalloys have been widely used for the blades and other loaded structures of aero-engines and gas turbines due to their superior mechanical properties, in particular their excellent creep resistance at high temperatures [1]. Their outstanding creep resistance, not only origins from the absence of grain boundaries but is largely determined by the unique microstructure characterised by the presence of a high-volume fraction of the long-range ordered $L1_2$ γ′ phase, which appears as cubes coherently embedded in a face-centered cubic solid solution γ matrix. In general, the size, volume fraction and morphology of γ′ precipitates mainly determine the mechanical properties of Ni-superalloys [2,3]. In the as-produced condition the cuboidal γ′-precipitates have a size of around 0.4um size and they are separated by γ-channels with around 0.1um size. The typical precipitate volume fraction at room temperature is 50 % or higher [1].

When exposed to their typical use conditions, a relatively high temperature (>950 °C) and a modest stress (<250 MPa), there is directional coarsening of γ′ precipitates during the early creep stage, which is so-called "rafting" stage [4–7]. During this time, the initially adjacent cuboidal γ′ particles coalesce and form platelets that turn into plate-like or rod-like structures. This lamellar γ/γ' rafted microstructure will remain more or less unchanged during the long stable creep stage, until the γ' gradually interconnects and becomes the matrix phase surrounding isolated γ phase islands [8,9]. This process is known as the 'topological phase inversion', which has been considered as the microstructural indicator marking the transition from quasi-stationary creep to accelerated creep. This inverted microstructure is maintained during the accelerated creep stage but rapidly loses it regularity, the morphology evolution of the phases during the entire creep life is presented in Fig. 1 [10].

On the other hand, the creep response not only depends on the microstructure evolution but also on the changes in the dynamics and topology of the dislocations and dislocation networks [11]. At the beginning of creep loading, the deformation is governed by the dislocation glide and dislocation multiplication in the γ channels. Soon thereafter the mobile dislocations start to accumulate and become rearranged at the γ/γ' interface, while the formation of lamellar rafts takes place, leading to the widely observed formation of dislocation networks on the γ/γ' interface [11–15]. Analogous to the lamellar microstructure, the dislocation network will remain stable until the end of the stable creep stage (stage II creep) when the network begins to degrade by huge amounts of dislocations cut-

* Corresponding author at: Novel Aerospace Materials Group, Faculty of Aerospace Engineering, Delft University of Technology, 2629HS, Delft, the Netherlands.
*E-mail address:* xuwei@ral.neu.edu.cn (W. Xu).

https://doi.org/10.1016/j.jmst.2019.11.028
1005-0302/

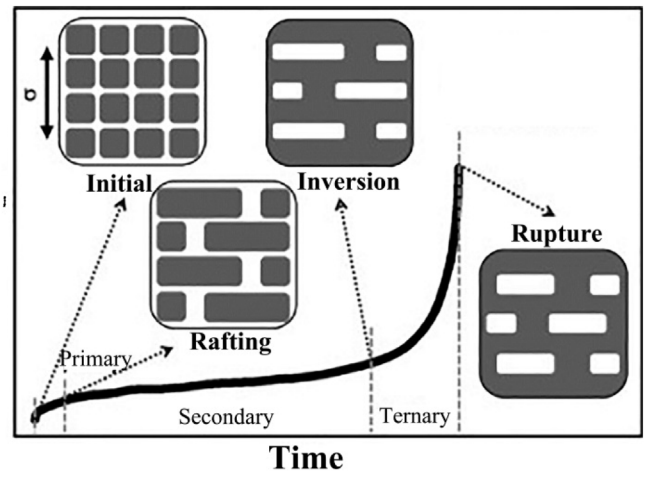


**Fig. 1.** Schematic illustration of the microstructure evolution of Ni superalloy single crystals during high temperature low stress creep loading. The black phase is the $\gamma'$ phase, while the white phase marks the $\gamma$ phase. The stress is applied in the direction parallel to the *y*-axis [10].

ting into the rafted $\gamma'$ through the interface. Ultimately this chaotic dislocation multiplication process leads to rupture.

Summing up, the creep properties of Ni single crystal superalloys are strongly dependent on the combined effect of the microstructure evolution and the dislocation behaviour. Therefore, a good understanding and some quantification of microstructure and dislocation evolution during creep is crucial to better comprehend the mechanical properties of Ni superalloys. In this work, the current work on the dependence of mechanical properties in Ni single crystals on the microstructural and dislocation behaviour during isothermal creep tests is reviewed. The experimental observations and the corresponding models and simulations are combined to show their mutual interaction. A simple model has been built in which the governing dislocation dynamics equation is thermodynamically coupled to the chemical composition of some commercial superalloys to predict their minimum creep rate at the loading conditions.

## 2. Microstructure evolution

### 2.1. Initial microstructure

The $\gamma'$ precipitates in Ni superalloys undergo a succession of morphology changes from spheres to cubes during the heat treatments preceding the actual use phase. At the very beginning, the $\gamma'$ precipitates nucleate as spheres to minimize the surface area [16]. As the particles grow, the misfit strain energy induced by the lattice and modulus mismatch between the $\gamma$ and the $\gamma'$ phase increases, and the precipitates become cuboids as the reduction in strain energy more than compensates for the increase in surface energy. It has been proven that cube morphology best minimizes the total energy of the precipitate as it provides the best balance between the anisotropic strain energy and the isotropic interfacial energy [17].

Nathal [18] has quantitatively investigated the optimal size of initial (i.e. as produced) particle and his work shows that alloys with an initial $\gamma'$ particle size between 0.35 and 0.5 $\mu$m can pronouncedly outperform their counterparts with the same level of particle volume fraction but a different initial particle size. Hence the optimal initial microstructure consists of aligned cuboidal $\gamma'$ particles with a size around 0.4 $\mu$m. This value of size has been widely adopted as the typical dimension of initial $\gamma'$ particles for most of the commercial Ni superalloys. To explore the possible "optimal" volume fraction of $\gamma'$ phase, Murakumo et al. started their study based on TMS-75 single crystal superalloy [2]. Results show that the dependence of the creep rupture life on the amount of $\gamma'$ was more evident in single crystals than in polycrystals, while the "optimal" amount of $\gamma'$ phase which leads to the longest creep lifetime is not a constant and varies with different service temperature. In some design models of Ni superalloys [19,20], the optimal volume fraction of $\gamma'$ phase at different temperatures was generally set around 50 %, which was mainly due to the dependence of topological inversion on the $\gamma/\gamma'$ volume.

### 2.2. Rafting stage

Rafting is one of the most pronounced characteristics of high temperature creep deformation in nickel-based superalloy single crystals [5,7,21,22]. During creep tests at a high temperature and a low unidirectional applied stress, the microstructure in Ni superalloys gradually degrades by a directional coarsening process of $\gamma'$ precipitates. The initially adjacent cuboidal $\gamma'$ particles coalesce and form platelets that turn into plate-like or rod-like structures. The orientation of directional coarsening is closely related to the driving force of rafting, which is proportional to the product of applied stress and the lattice misfit [7,23]. For negative misfitting alloys (where the lattice parameter of $\gamma'$ precipitates is smaller than that of $\gamma$ matrix), N-type coalescence is observed (i.e. rafts form normal to the direction of the applied stress) during tensile creep test, whereas P-type coalescence is obtained in compressive loading (i.e. rafts form parallel to the direction of the applied load). Conversely, for alloys with positive lattice misfit, the tensile loading leads to P-type coalescence and vice versa. Describing the morphological change in microstructure dimensions during rafting is a direct way to understand the evolution of mechanical properties.

To quantify the kinetics of rafting process, the key microstructural parameters presenting the morphology change need to be extracted and characterised. The $\gamma$ channel widening is an important process during the creep seen in microstructures evolution, since $\gamma$ channels are the conserved domains where dislocations propagate and glide during primary creep. Kamaraj et al. investigated the kinetics of the widening of $\gamma$ channels in the $\gamma/\gamma'$ microstructure, whose result suggests that multi-atom diffusion through the $\gamma$ channels controls the widening process [24]. Later work by Serin et al. further explored the effect of the level and state of applied stress on the kinetics of $\gamma$ channel widening [25]. Results shown that <100> tension and (011)<01 $\bar{1}$ > shear creep deformation can equivalently lead to the same microstructure evolution, while $\gamma$ channel widening rates increase with increasing stress level.

The structural periodicity $\lambda$ in Ni superalloys is another important microstructural parameter and this is defined as the sum of the width of the N-channels and the extent of the $\gamma'$ phase in the direction parallel to applied stress [26]. This parameter characterizes the global coarsening of $\gamma/\gamma'$ microstructure since $\gamma/\gamma'$ composite morphology is almost periodical both for the initial microstructure and for the fully rafted microstructure [27]. This work indicates that the microstructure period $\lambda$ does not change remarkably during rafting, which means that rafting in essence is an anisotropic coarsening process. The growth of $\gamma'$ cuboids, characterized by the first increase in $\lambda$, precedes the coalescence of $\gamma'$ cuboids into rafts taking place without a great change in $\lambda$.

Rafting is generally considered as a creep hardening process, since the morphological change in $\gamma/\gamma'$ in fact retards the evolution of creep strain [28–30]. Reed et al. attributed this hardening effect to the closure of vertical $\gamma$ channels during the morphology change [31]; the movement of dislocations contributing to the deformation creep is hindered by the lamellar structure with the orientation

normal to the applied stress, leading to dislocation accumulation and rearrangement on the γ/γ' interface [12,13].

### 2.3. Stable post-rafting stage and topological inversion

Generally, the rafting process is terminated at or before the stable creep stage. The fully rafted lamellar γ/γ' microstructure can hereafter maintain their morphology for a relatively long time, with only minor coarsening behaviour of γ' plates taking place [27,32]. This stable post-rafting controls the microstructural dynamic recovery process, leading to a very slow accumulation of creep deformation.

At the end of creep stable stage with a sufficient time for the rearrangement of the lamellar morphology, the γ' phase gradually interconnects and is no longer confined by the γ channels. This evolution leads to an effect called "topological inversion": the γ' phase now surrounds the γ phase and topologically becomes the matrix [8,33–36]. The moment of topological inversion has been proven to be strongly dependent on the initial volume fraction of γ' phases [37]. The reason for the formation of inversed microstructure has been studied in detail by many researchers [8,9,37]. It is generally accepted that after the rafting stage, the misfit stresses on γ/γ' interface are released by the dislocation network, and then the γ' precipitate size and morphology will evolve such as to minimize the total interfacial energy. This evolution is obtained by a reduction in γ/γ' interface area driven by diffusion-controlled coarsening of the γ particles. For the modern Ni single crystal superalloys with a typical γ' fraction greater than 50 % at service temperature, the topological inversion of the γ/γ'microstructure is due to the minimization of the total γ/γ' interface area with the minor phase embedded in the major one. The occurrence of topological inversion is generally seen as the indicator of onset of accelerated creep [8,36].

### 2.4. Break-up stage

After the inversion of the γ/γ' microstructure, the creep resistance degrades, rapidly which finally leads to the failure of superalloys. Mughrabi ascribes this deterioration to a rapid increase in deformation induced by internal stresses, which cannot be released any longer by the interface dislocations once the γ phase is being split into discrete islands [38]. Other studies [33,39,40] have indicated that in the inversed microstructure the shape of γ/γ' interfaces changes from smooth into zigzag, leading to the formation of new dislocation glide planes in γ', which correspondingly promote the formation of dislocation pile-ups and consequently cutting of the γ' phase.

### 2.5. Modelling of microstructure evolution

To interpret and further predict the directional coarsening behaviour of Ni superalloys, a large number of models have been proposed [32,41–56]. Emphasis has been put on explaining the orientation of rafting based on driving force of morphology variation. Andre explains the behaviour in an elastic framework, where the elastic energy is calculated as a function of the particle shape, the applied stress and the ratio between the Young's modulus of the precipitates and that of the matrix [41]. The influence of plastic strains was added by considering the effect of unevenly distributed interfacial dislocations. Meanwhile the anisotropy in releasing the coherency stresses have been also simulated [42–44]. The original local stresses induced by the lattice and modules mismatch distributed evenly in γ matrix. When the external stresses were applied on the materials, the local state of stress in γ/γ' microstructure has been modified, which lead to anisotropic coarsening behaviours. The orientation dependence of elastic energy for different morphologies was then quantified for the combinations of transformation strain and matrix plastic strain [45]. These abovementioned models have pointed out that driving forces on rafting are in essence the lattice misfit, the external loading, and the difference in elastic constants between the two phases.

Besides, other studies focused on quantitatively describing the kinetics of the morphology changes during rafting. Svodoba's model takes into account the interactions between dislocations and channels of γ matrix [46]. Through modelling the coarsening behaviour of γ' particles, the intricate creep behaviour can be well captured. Fedelich and co-workers made systematic studies to quantify the microstructural parameters of commercial alloy CMSX-4 during rafting process [32,47,48]. The direction widening behaviour of γ channel width is perfectly fitted as a function of time, stress and temperature, and the morphology description was further applied to build the constitutive model by connecting with creep properties [49].

Recently, the phase field method has emerged as a powerful way to capture the morphology change in Ni superalloys. Early phase field models were based on a elasticity framework only [50,51], while the contributions from plastic strains were introduced in later models [52–54]. The principal criteria in all abovementioned models remain the lattice misfit, the elastic inhomogeneity and the applied load as the driving force for the directional coarsening. The effects of diffusion on the kinetics of rafting have been studied by coupling the phase field calculations with a CALPHAD approach [55,56]. Results elucidate that Re addition retards the kinetics of rafting by slowing down the mobility of γ/γ' interface.

## 3. Evolution of dislocation structures

### 3.1. Dislocations in initial microstructure

For the commercial Ni single crystal superalloys with the typical microstructure of aligned cubic γ' embedded in γ matrix, the well-organized γ/γ' coherent initial microstructure is obtained by a multi-step solution and aging treatment followed by a slow air-cooling process. The density of dislocations in the initial microstructure will be at a sufficiently low level after the high-temperature heat treatment and the as-processed γ/γ′ microstructure can be approximately considered as a dislocation-depleted state.

When the stress is applied during the early stages of creep, the dislocations are primarily emitted from the low-angle boundaries and percolate into the narrow γ channels. As creep deformation proceeds, the mobile individual dislocations become sequentially active and start to generate short avalanches of creep dislocations in boundary-free regions. Upon their activation, the density of creep dislocations in boundary-free regions rises by two orders of magnitude. Experimental observation at this stage shows that the γ/γ′ interfaces parallel to the applied stress are nearly devoid of dislocation, while dislocations are frequently observed on the γ channels normal to the stress axis [13]. The anisotropic distribution of dislocations in different γ channels is ascribed to the effect of unidirectional applied stress, which releases the misfit strain in parallel channels while introducing higher strains in the transverse channels [14,57]. The deformation mechanism during primary creep has been generally interpreted as the rapid growth in dislocation density and the filling of γ channels with dislocations [33,58,59].

### 3.2. Formation of interfacial dislocation network

As the microstructure turns into rafts, the dislocations will accumulate at the γ/γ′ interfaces and form planar dislocation networks. It is commonly reported that networks form by the reaction

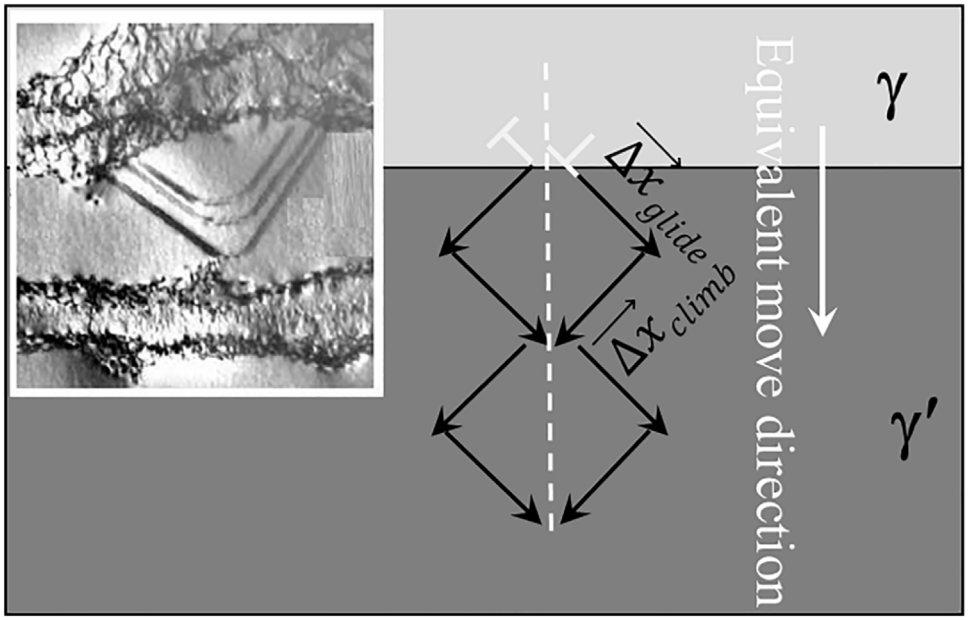


**Fig. 2.** 2D sketch for the superdislocations cutting into γ'rafts [70].

of two dislocations with same Burgers vector to rearrange and generate new dislocations [14,60–62], while Eggerler and Dlouhy also observed the formation of new dislocations on γ/γ' interface contributed by the interaction of two dislocations with different Burgers vector [63]. The formation of interfacial dislocations is usually believed to be driven by the release of lattice mismatch strain between the γ' precipitate and γ matrix [12,13]. The magnitude of lattice misfit is therefore of vital importance in the sense of determining the formation of the dislocation network. Zhang et al.'s experimental results [64] provide direct evidence for the dislocation networks evolution due to lattice misfit. In alloys with a large negative lattice misfit, the dislocations rearrange in the γ channels and form more complete and condensed dislocation networks and at a higher speed than in alloys with a small misfit Harada and coworkers [65] have isolated a quantitative correlation between the dislocation density of the equilibrium network and their creep performance in single crystal, with the dislocation spacing being found to be proportional to the logarithm of the minimum creep rate. The positive correlation between creep strength and interfacial dislocation density was also proven by Zhang et al.'s work [66]. Basically, the formation of interfacial dislocation network helps to release the γ/γ' misfit strain, meanwhile contributes to the strengthening mechanism of γ/γ' lamellar structure by hindering the cutting the mobile dislocations in the matrix.

### 3.3. Sustenance of the stable dislocation network

Experimental observations have shown that the networks can maintain their morphology and density during the secondary creep stage [62,67,68]. As mentioned above, the interfacial dislocation network can act as dislocation sinks to absorb/accommodate the matrix dislocations, thereby effectively preventing matrix dislocations from piling up at the interface [69]. Moreover, the dislocation networks also provide dislocation pins to prevent the matrix dislocations from cutting into the γ′ precipitate [11]. The stability of dislocation network helps to correspondingly stabilize the lamellar γ/γ' structure during the stable creep stage. So clearly there is mutual stabilisation.

The stable stage for γ/γ' interfacial dislocation network corresponds to the creep stable stage, which presents the microstructural dynamic recovery process with a very slow accumulation of creep deformation. Srinivasan investigated the recovery behaviour of mobile dislocations, focusing on the mechanism of γ' rafts cutting [70]. Experimental observations show that two dislocations with different Burgers' vectors in γ channel jointly shear the γ' phase by forming a non-compacted superdislocation during [001] tensile creep. The two superpartials move into the γ' phase by a combined process of glide and climb, which is equivalent to the migration of single superdislocation. The 2D schematic illustration is shown in Fig. 2. Similar results were proved by experiments from many other researches [71–74], while the superdislocation-cutting-γ' mechanism has been widely accepted as the dominate recovery mechanism during creep stable stage. According to this climb-plus-glide cutting process, the rate-controlling step in creep is essentially the climb rate of dislocations in γ'.

In addition, Epishin and Link proposed another mechanism for dislocation movement during stable creep [33]. Here dislocations in the γ channels segregate on γ/γ' interface during primary creep, then move transversely to the applied stress by a combination of glide and climb, while the gliding dislocations first get pinned by γ' rafts. But with the help of osmotic forces produced by temperature and stress, trapped dislocations can climbs away from its original slip plane. Then the climbing dislocation can glide in a new slip plane again once its climb distance is large enough to afford a new glide step before it is blocked again by γ' rafts. The 2D sketch of dislocation movement is shown in Fig. 3. As a result, the dislocations in the matrix channels can move along the γ/γ' interface in a zig–zag manner as shown in the figure. Unlike the collective shearing of γ' rafts, dislocations in this mechanism are compact, and migrating only in γ matrix. A similar description of the dislocation migration on γ/γ' interfaces can also be found in Refs. [75,76].

### 3.4. Break-up of interfacial dislocation structure

The γ/γ' microstructure becomes inversed when creep enters the tertiary stage. A large part of the dislocation network is still present on the γ/γ' interfaces, but some are locally damaged in a later period of creep. The damaged networks lose the co-ordinating role of maintaining the dynamic equilibrium, so

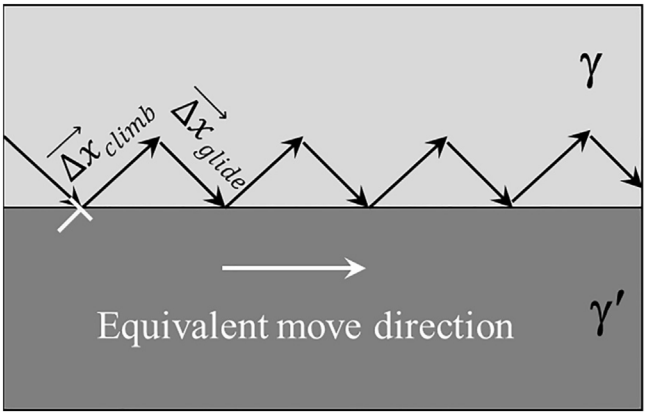


**Fig. 3.** 2D sketch for the motion of a dislocation on γ/γ' interface [75].

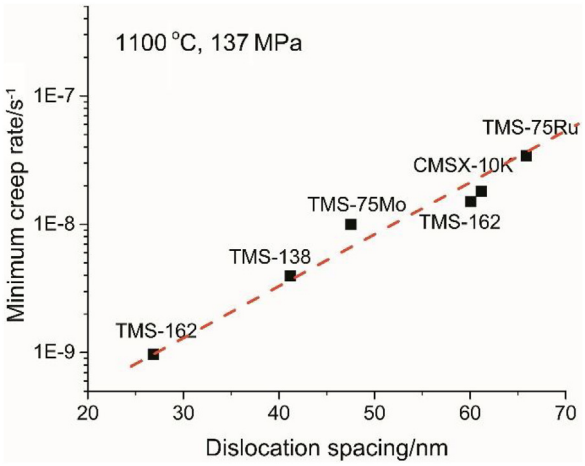


**Fig. 4.** The minimum creep rate of commercial Ni single crystal superalloys as a function of interfacial dislocation spacing during 1100 °C, 137 MPa creep [11,57,65].

that a large number of dislocations are piled up at some regions where the networks have been damaged, giving rise to the local stress concentration [14]. Experimental results have shown that the {111}-type distorted interface forms as a consequence of the inversed microstructure [73,74,77]. The zigzag interface forms through dislocations which cut into the γ'raft via {111} planes of interface [40]. The accelerated creep rate can then be attributed as the increased dislocation activity with the break-down of dislocation networks and the formation of new gliding planes.

### 3.5. Modelling the dislocation evolution

Based on a constitutive model for precipitate-strengthened alloys from Dyson [78], Zhu et al. has developed a model by simulating the interaction between the dislocation and the γ' particles with a cuboid morphology [76]. The rate-controlling step is assumed to be climb of dislocations at the matrix/particle interface, hereby the creep rate can be modelled as a function of microstructural parameter as well as intrinsic dislocation diffusivity.

At the mesoscopic scale, the main computational tool to study the dynamic collective evolution of dislocations under the external loading is discrete dislocation dynamics (DDD) simulation. The application of DDD in Ni superalloys was primarily concerned with superdislocations in the γ' phase, focusing on the role of cube size and shape, phase volume fraction, temperature and anti-phase boundary energy [79–81]. Attention has been paid to the rafting domain to tackle dislocation plasticity in γ channels of γ/γ' microstructures, which makes dislocation climb and vacancy diffusion become unavoidable key issues. In Hafez Haghighat et al.'s work, the movement of dislocations along the γ/γ′ interface close to the γ'cube was interpreted as a combination of dislocation glide and climb, while the net dislocation motion is climb controlled [82]. Work done by Gao et al. explicitly takes into account the vacancy-diffusion-coupled dislocation climb, which shows that dislocation climb can rearrange the dislocation configuration to relax the hardening due to dislocation filling γ channels [83]. Yang et al.'s work also puts emphasis on simulating the diffusion-induced dislocation climb to study the primary creep and early plastic behaviour [75]. The influences of microscale vacancy supersaturation and mesoscale phase morphology were described in detail. Using a DDD model, the effect of interfacial diffusion on the creep behaviour has been investigated by Shishvan et al. [84]. Results show that interfacial diffusion helps to rearrange the dislocation distribution, as well as to relax the back-stresses induced by dislocations pile-up. The DDD model has also been combined with finite element method by Song to investigate the influence of interfacial dislocation networks and lattice mismatch on the dynamics of dislocation evolution in the matrix channels [85].

## 4. Discussion

### 4.1. The dependence of minimum creep rate on interfacial dislocation density

As shown in Fig. 4, the minimum creep rate of commercial Ni single crystal grades increases linearly with the spacing of the interfacial dislocations [11,57,65]. This phenomenological relationship can give an intuitive first-order connection between the creep properties and the dislocation properties. However, the parameter dislocation spacing is highly dependent on the accuracy of experimental observation. Moreover, the application of this relationship to quantify the creep behaviour of existing superalloys or further predict the properties of novel superalloys, is largely infeasible. To build a constitutive relationship with physical meanings instead of fitting equations, more detailed description in the dependence of dislocation behaviour needs to be made, while the dislocation-behaviour-based deformation mechanism needs to be taken into consideration.

### 4.2. Simulation of dislocation behaviour

Formal statements have shown that the layered fully-rafted structure coupled with γ/γ′ interfacial dislocation network can remain stable and keep almost unchanged for a relatively long time until rupture. Therefore, the investigation of creep properties as the dependence of dislocation behaviour should be focused on the post-rafting stage as the most long-lasting stage. As stated before, Srinivasan et al.'s research has shown that the γ' rafts can be cut by the superdislocation through a combined process of glide and climb, where the climbing velocity of superpartials are the controlling factors of creep rate [70]. The following discussion about creep is by default referred to the [001] tensile creep. Based on this results, the classic dislocation climb model from Anderson et al. [86] was employed as a first order approximation to estimate the dislocation mobility, where the climbing rate of dislocations in γ' phase $v_{c'}$ has been presented as follows:

$$v_{c'} = \frac{2\pi D_{s'}\left(e^{\frac{\sigma_{xx}V_{a'}}{kT}} - 1\right)}{b\ln(R'/b)} \tag{1}$$

where $D_{s'}$ is the diffusivity of γ′, $\sigma_{xx}$ is the applied stress, $V_{a'}$ is the atomic volume of γ′, $b$ is the Burger's vector, $R'$ is the average dislocation spacing in γ′ and $R' \approx \sqrt{1/\rho_{\gamma'}}$, and $\rho_{\gamma'}$ is the dislocation density in γ′ phase.

For the dislocation zig-zag movement along the γ/γ′ interface proposed by Epishin and Link [33], the creep rate controlling factor of this mechanism is similarly the dislocation climb rate. Here the compact dislocations move along γ/γ′ interface without superpartials, and the γ matrix is the domain of dislocation migration. Anderson et al.'s theory was again employed [86], and the climbing rate of dislocation on γ/γ′ interface was shown as follows:

$$\boldsymbol{v_c} = \frac{2\pi \boldsymbol{D_s}(\mathrm{e}^{\frac{\sigma_{xx}V_a}{kT}} - 1)}{\boldsymbol{b}\ln(\boldsymbol{R}/\boldsymbol{b})} \quad (2)$$

where $D_s$ is the diffusivity of γ, $V_a$ is the atomic volume of g, $R$ stands for the average distance of dislocations on the γ/γ' interface. The interfacial dislocation density of Ni superalloys has been reported by many researchers as a function of lattice misfit [68], where the spacing of dislocation network $R = |b|/|\delta|$. Here $\delta$ is the lattice misfit presenting by $\delta = \frac{a_{\gamma'} - a_\gamma}{a_\gamma}$. $a_{\gamma'}$ and $a_\gamma$ are the lattice parameter of γ' and γ phase, respectively. So the equation was represented in the following way:

$$v_c = \frac{2\pi D_s(\mathrm{e}^{\frac{\sigma_{xx}V_a}{kT}} - 1)}{-b\ln|\delta|} \quad (3)$$

In this work, the lattice misfit is obtained, from the lattice parameters of γ/γ′ phases calculated through their molar volumes $a = \sqrt[3]{\frac{4V_m}{N_A}}$. For the calculation of diffusion coefficient in the multi-element alloy system, a harmonic mean of calculation is selected based on Zhu et al.'s work [76], i.e., $D_s = 1/\sum_m \frac{x_m}{D_0^m}$.

By now the creep rate-controlling behaviours of dislocations in γ and γ′ phase have been presented respectively. After figuring out the underlying deformation mechanism originating from dislocation behaviour, the creep behaviour of superalloys can be then interpreted as the combination of these two mechanisms.

### 4.3. Simulation of minimum creep rate

For the fully rafted γ/γ′ lamellar microstructure, the creep behaviour can be approximately equal to the composites reinforced by the continuous lamellae, which are oriented perpendicular to the applied stress. Assuming an iso-stress condition [87], the strain rate of alloy can be presented by the following equation:

$$\dot{\boldsymbol{\varepsilon}} = \dot{\boldsymbol{\varepsilon}}_{\boldsymbol{\gamma}}\boldsymbol{V_\gamma} + \dot{\boldsymbol{\varepsilon}}_{\boldsymbol{\gamma}}\boldsymbol{V_{\gamma'}}, \quad (4)$$

where $V\gamma$ and $V\gamma'$ are the volume fraction of γand γ′ phase respectively. According to the Orowan law, the strain rate in g and g' phase can be written as:

$$\dot{\boldsymbol{\varepsilon}}_{\boldsymbol{\gamma}}\dot{\boldsymbol{\varepsilon}}_{\boldsymbol{\gamma}} = \overline{\boldsymbol{M}}\boldsymbol{\rho_\gamma}\boldsymbol{b}\boldsymbol{v_c} \quad (5)$$

where $\rho_\gamma$ stands for the dislocation density in γ; and $\overline{M}$ is the Schmid factor.

However, the abovementioned equation describes the creep properties of alloys with a lamellar microstructure without taking into consideration the distribution of lamellae spacing, and the effect of inter-spacing of lamellae need to be further interpreted. Whitely proposed a model based on the Bailey-Norton creep equation to describe Al-$CuAl_2$ eutectic alloy with lamellar structure [88], where dislocation-motion related microstructural parameter, inter-lamellar spacing L, was added, as shown by the following equation

$$\dot{\boldsymbol{\varepsilon}} \propto \boldsymbol{L^n} \quad (6)$$

where $n$ is the lamellar spacing exponent. Theoretically n should be equal to 1 for a perfectly aligned and continuous fiber (or plate) reinforced composite, but it will be as high as 3 if fiber (or plate) rupture occurs. The application of equation can also be found [89,90] with similar well-aligned lamellar structure. In this work the lamellar inter-spacing can be defined as the channel width of γ′ phase to present the periodical microstructure. According to the geometrical relationship, L can be expressed in the following way:

$$L = \frac{V_{\gamma'}}{1 - V_{\gamma'}{}^{1/3}}\omega_0 \quad (7)$$

where $\omega_0$ is the initial size of γ′ particles.

Combining all, the creep rate can be expressed by the following equation:

$$\dot{\varepsilon} = L^n\left(\frac{2\pi\overline{M}V_{\gamma'}\rho_{\gamma'}D_s'\left(\mathrm{e}^{\frac{\sigma_{xx}V_a'}{kT}} - 1\right)}{\ln\left(\frac{R'}{b}\right)} - \frac{2\pi\overline{M}\rho_\gamma V_\gamma D_s(\mathrm{e}^{\frac{\sigma_{xx}V_a}{kT}} - 1)}{\ln|\delta|}\right) \quad (8)$$

The creep properties of Ni superalloys can be presented by dislocation behaviour through building the climb-assisted equation with the consideration of lamellar microstructure. In equation, the parameters such as phase volume fraction $V\gamma$ and $V\gamma$', diffusivity $D_s$ and $D_s'$, and lattice misfit $\delta$ are thermodynamic factors that are strongly related to chemical composition. The mechanical properties of superalloys can be then connected with the composition when these thermodynamic parameters can be properly obtained as a consequence of composition. While the model as given by Eq. (8) is probably conceptually correct, the large number of physical parameters which values cannot be obtained independently, implies that the model cannot easily be used for the compositional optimisation of existing alloys, nor the design of new superalloys.

In the field of superalloys, the implementation of CALPHAD-based thermodynamic models is now an emerging approach, where equilibrium microstructural features of complex multi-component alloys, such as phase fraction, element partition and diffusivity, can be well captured by using Gibbs free energy databases. Values for the parameters such as $V_f$, $V_m$, $x_m$, $D_s$ were calculated via Thermo-Calc using TCNI9 and MOB2 database. Since the minimum creep rate is also a function of the (a-priori unknown) dislocation density in γ and γ' phase in the following simulations it was pre-set as a constant. This is a slight simplification but helps us to illustrate the effect of composition-related factors. The microstructural parameters and physical constants used in equation are listed in Table 1 [70,76].

**Table 1**
Microstructural parameters and physical constants used in equation [70,76].

| Parameter | Value |
|---|---|
| Lamellar spacing exponent, $n$ | 1.5 |
| Schmid factor, $\overline{M}$ | $1/\sqrt{6}$ |
| Burger's factor, $b$ | $2.5 \times 10^{-10}$ m |
| Dislocation density in γ' phase, $\rho_{\gamma'}$ | $10^9$ m$^{-2}$ |
| Dislocation density in γ phase, $\rho_\gamma$ | $10^{11}$ m$^{-2}$ |
| Initial size of γ' particles, $\omega_0$ | $4 \times 10^{-7}$ m |

### 4.4. Validation of minimum creep rate in existing Ni commercials

To illustrate the model's capability in reproducing the creep properties of superalloys, existing commercial grades of Ni single crystals have been employed with their chemical compositions shown in Table 2. Based on the composition, the volume fraction as well as the diffusivity of γ and γ′ phase in existing alloys at 1100 °C are calculated and shown in Fig. 5.

In Fig. 5(a), the square dots with black and grey colour indicate the calculated diffusion coefficient in γ and γ′ phases respectively. For all alloys, almost no difference can be found in the diffusivity of γ′ phase, due to the relatively small solubility of alloying ele-

**Table 2**
Chemical compositions of commercial Ni single crystal superalloys (wt%) [65,77,91–94].

| Sample | Al | Co | Cr | Hf | Mo | Re | Ru | Ta | Ti | W | Ni |
|---|---|---|---|---|---|---|---|---|---|---|---|
| TMS-75 | 6 | 12 | 3 | 0,1 | 2 | 5 | – | 6 | – | 6 | Bal. |
| CMSX-4 | 5,6 | 9 | 6,5 | 0,1 | 0,6 | 3 | – | 6,5 | 1 | 6 | |
| ERBO/39 | 4,4 | 8,92 | 5,11 | – | 0,97 | – | – | 6,7 | 3 | 9 | |
| ERBO/38 | 5,54 | 8,71 | 5,12 | – | 0,95 | – | – | 6,54 | 0,79 | 9,05 | |
| ERBO/37 | 6 | 8,74 | 5,14 | – | 0,95 | – | – | 6,56 | – | 9,09 | |
| ERBO/36 | 5,65 | 8,89 | 5,23 | – | 0,96 | – | – | 6,67 | – | 6,19 | |
| ASTRA100 | 6,13 | 8,92 | 5,25 | – | 0,97 | – | – | 6,7 | – | 6,19 | |
| CMSX-10K | 5,7 | 3 | 2 | 0,03 | 0,4 | 6 | – | 8 | 0,2 | 5 | |
| TMS-138 | 5,9 | 5,9 | 2,9 | 0,1 | 2,9 | 4,9 | 2 | 5,6 | – | 5,9 | |
| TMS-162 | 5,8 | 5,8 | 2,9 | 0,1 | 3,9 | 4,9 | 6 | 5,6 | – | 5,8 | |
| LSC-15 | 4 | 6 | 7 | 0,1 | 1,5 | – | – | 5,5 | – | 10 | |
| SX-0Ru | 6 | – | 4 | – | 1 | 4 | 0 | 5 | 0,5 | 5 | |
| SX-2Ru | 6 | – | 4 | – | 1 | 4 | 2 | 5 | 0,5 | 5 | |
| SX-4Ru | 6 | – | 4 | – | 1 | 4 | 4 | 5 | 0,5 | 5 | |

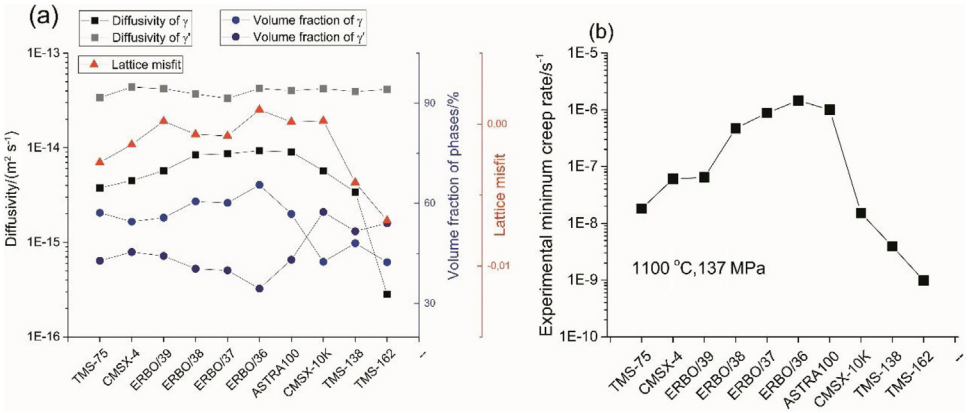


**Fig. 5.** Calculated diffusivity and volume fraction of γ and γ' phase, as well as the lattice misfit of existing Ni single crystal grades at 1100 °C (a) and the experimental minimum creep rates of alloys at 1100 °C, 137 MPa [65,91,92] (b). The lines connecting the individual data points have no physical meaning and are only added to guide the eye. The order of the superalloys along the *x*-axis is based on the generation of Ni commercial single crystal superalloys.

ments in the $Ni_3Al$ intermetallic. In comparison, the diffusivity in TMS-138 and TMS-162 alloys is significantly smaller than that in the other alloys, which is understandable due to the more heavily alloying by refractory elements (such as Re and Mo) in TMS series. Also, the calculated results demonstrate that difference of diffusivity in γ′ is small but that in γ is big, which implies the diffusion behaviour in γ phase is the dominate mechanism in deformation which leads to the difference in creep behaviour for Ni commercial grades. The round dots present the phase volume fractions of listing alloys, where ASTRA100, ERBO/36, ERBO/37 and ERBO/38 alloys have a relatively low values of γ′ volume fraction around 35 %. The red triangle dots show the calculated lattice misfits of all alloys. The TMS alloys generally possess large negative misfits, while the lattice mismatch of other alloys fluctuates around zero with small difference. Fig. 5(b) shows the experimental minimum creep rates of these alloys at 1100 °C and 137 MPa. TMS-162 alloy pronouncedly outperforms other alloys while ERBO/36 has the worst performance in creep. The influence factors corresponding to the composition-related parameters have been analysed.

Fig. 6 shows the comparison between the experimental minimum creep rates of existing Ni grades, and the calculated minimum creep rates obtained from thermodynamic simulations. The selected experimental data are obtained from different temperature and stress ranges [65,77,91–94]. Results show that compared to the experimental results, the creep rates are generally overestimated by the simulations, as indicated by the red dash line. But it is worth pointing out this model based on the simulation of dislocation movement can well reproduce the creep properties of existing Ni superalloys at different temperature and stress ranges. Hence, through thermodynamic and kinetic calculations, the chemical compositions of Ni superalloys can be successfully coupled to their creep performance by this model without making the dislocation specifications themselves composition dependent.

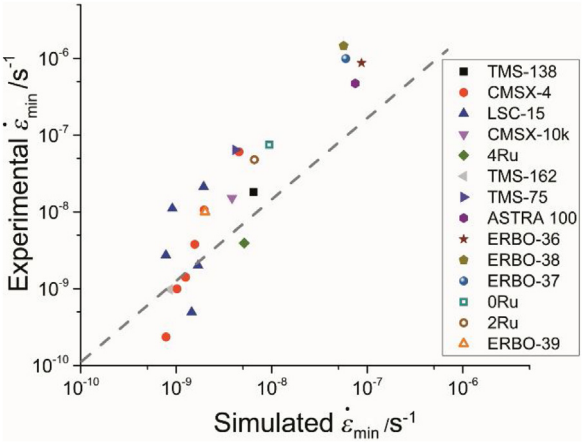


**Fig. 6.** Simulated minimum creep rate of existing Ni commercial grades compared with the experimental results obtained from the literature [65,77,91–94].

## 5. Conclusions

(1) The high performance of Ni single crystal superalloys during high temperature low stress creep service, is primarily controlled by the combined effects of microstructural evolution, namely the formation of rafting lamellae, and the dislocation

behaviour, i.e., the well-arranged dislocation network located on the γ/γ′ interface.

(2) During the secondary creep stage which takes longest time of creep life, two main recovery mechanism based on dislocation migration dominate the process. One is superdislocations shearing into γ' rafts through a two-superpartials-assisted approach. Another is the compact dislocations migrating along γ/γ′ interface. These two mechanisms are similarly climb-rate-controlled process.

(3) A model for the minimum creep rate based on thermodynamic and kinetic calculations and using an existing detailed dislocation dynamics model has been built by taking the dislocation migration behaviours as well as the rafted microstructure into consideration, which can well reproduce the creep properties of existing Ni superalloy grades.

## Acknowledgements

This work was financially supported by the National Natural Science Foundation of China (No. 51722101) and the Key Research and Development Project (No. 2017YFB0703001).

## References

[1] R.C. Reed, The Superalloys: Fundamentals and Applications, Cambridge University Press, Cambridge, 2008.
[2] T. Murakumo, T. Kobayashi, Y. Koizumi, H. Harada, Acta Mater. 52 (2004) 3737–3744.
[3] L. Shui, T. Jin, S. Tian, Z. Hu, Mater. Sci. Eng. A 454–455 (2007) 461–466.
[4] R.A. Ricks, A.J. Porter, R.C. Ecob, Acta Metall. 31 (1983) 43–53.
[5] W. Johnson, M. Berkenpas, D. Laughlin, Acta Metall. 36 (1988) 3149–3162.
[6] S. Socrate, D.M. Parks. Acta Metall. Mater. 41 (1993) 2185–2209.
[7] F.R. Nabarro, Metall. Mater. Trans. A 27 (1996) 513–530.
[8] A. Epishin, T. Link, U. Brückner, P. Portella, Acta Mater. 49 (2001) 4017–4023.
[9] J.V. Goerler, I. Lopez-Galilea, L.R. Mujica, O. Shchyglo, W. Theisen, I. Steinbach, Acta Mater. 124 (2017) 151–158.
[10] X. Tan, J. Liu, T. Jin, Z. Hu, H. Hong, B.G. Choi, I.S. Kim, C.Y. Jo, Mater. Sci. Eng. A 528 (2011) 8381–8388.
[11] J. Zhang, T. Murakumo, Y. Koizumi, T. Kobayashi, H. Harada, S. Masaki, Metall. Mater. Trans. A 33 (2002) 3741–3746.
[12] A. Lasalmonie, J. Strudel, Philos. Mag. 32 (1975) 937–949.
[13] T. Gabb, S. Draper, D. Hull, R. MacKay, M. Nathal, Mater. Sci. Eng. A 118 (1989) 59–69.
[14] S. Tian, J. Zhang, H. Zhou, H. Yang, Y. Xu, Z. Hu, Mater. Sci. Eng. A 279 (2000) 160–165.
[15] J. Zhang, H. Harada, Y. Koizumi, T. Kobayashi, J. Mater. Sci. 45 (2010) 523–532.
[16] R. Ricks, A. Porter, R. Ecob, Acta Metall. 31 (1983) 43–53.
[17] A. Baldan, J. Mater. Sci. 37 (2002) 2379–2405.
[18] M. Nathal, Metall. Trans. A 18 (1987) 1961–1970.
[19] Z. Zhu, L. Höglund, H. Larsson, R.C. Reed, Acta Mater. 90 (2015) 330–343.
[20] R. Rettig, N.C. Ritter, H.E. Helmer, S. Neumeier, R.F. Singer, Model. Simul. Mater. Sci. 23 (2015) 1–24.
[21] M. Kamaraj, Sadhana 28 (2003) 115–128.
[22] W.C. Johnson, Metall. Trans. A 18 (1987) 233–247.
[23] M. Ignat, J. Buffiere, J. Chaix, Acta Metall. Mater. 41 (1993) 855–862.
[24] M. Kamaraj, K. Serin, M. Kolbe, G. Eggeler, Mater. Sci. Eng. A 319 (2001) 796–799.
[25] K. Serin, G. Göbenli, G. Eggeler, Mater. Sci. Eng. A 387 (2004) 133–137.
[26] A. Epishin, T. Link, P. Portella, U. Brückner, Acta Mater. 48 (2000) 4169–4177.
[27] A. Epishin, T. Link, H. Klingelhöffer, B. Fedelich, U. Brückner, P.D. Portella, Mater. Sci. Eng. A 510 (2009) 262–265.
[28] H. Mughrabi, U. Tetzlaff, Adv. Eng. Mater. 2 (2000) 319–326.
[29] R.C. Reed, D.C. Cox, C. Rae, Mater. Sci. Technol. 23 (2007) 893–902.
[30] C. Rae, R. Reed, Acta Mater. 55 (2007) 1067–1081.
[31] R. Reed, N. Matan, D. Cox, M. Rist, C. Rae, Acta Mater. 47 (1999) 3367–3381.
[32] B. Fedelich, G. Künecke, A. Epishin, T. Link, P. Portella, Mater. Sci. Eng. A 510–511 (2009) 273–277.
[33] A. Epishin, T. Link, Philos. Mag. 84 (2004) 1979–2000.
[34] P. Caron, M. Benyoucef, A. Coujou, J. Crestou, N. Clement, ONERA, TP no 2000-230, 2000.
[35] A. Fredholm, J.L. Strudel, High Temperature Creep Mechanisms in Single Crystals of Some High Performance Nickel Base Superalloys, High Temperature Alloys, Springer, 1987.
[36] W. Walston, K. O'hara, E. Ross, T. Pollock, W. Murphy, Rene N6: third generation single crystal superalloy, in: Superalloy, 1996, pp. 27–34, Warrendale.
[37] P. Caron, C. Ramusat, F. Diologent, Superalloys, 2008, pp. 159–167.
[38] H. Mughrabi, γ/γ' Rafting and its effect on the creep and fatigue behaviour of monocrystalline superalloys, The Johannes Weertman Symposium (1996).
[39] T.M. Pollock, A.S. Argon, Acta Metall. Mater. 40 (1992) 1–30.
[40] Y. Ru, S. Li, J. Zhou, Y. Pei, H. Wang, S. Gong, H. Xu, Sci. Rep. 6 (2016) 1–9.
[41] A. Pineau, Acta Metall. 24 (1976) 559–564.
[42] D. Arrell, J. Vallés, Scr. Metall. Mater. 30 (1994) 149–153.
[43] J.Y. Buffiere, M. Ignat, Acta Metall. Mater. 43 (1995) 1791–1797.
[44] N. Matan, D. Cox, C. Rae, R. Reed, Acta Mater. 47 (1999) 2031–2045.
[45] N. Ratel, G. Bruno, P. Bastie, T. Mori, Acta Mater. 54 (2006) 5087–5093.
[46] J. Svoboda, P. Lukáš, Acta Mater. 46 (1998) 3421–3431.
[47] B. Fedelich, A. Epishin, T. Link, H. Klingelhöffer, G. Künecke, P.D. Portella, Comput. Mater. Sci. 64 (2012) 2–6.
[48] B. Fedelich, A. Epishin, T. Link, H. Klingelhöffer, G. Künecke, P.D. Portella, Rafting during high temperature deformation in a single crystal superalloy: experiments and modeling, in: Superalloys, 2012, pp. 491–500.
[49] T. Tinga, W. Brekelmans, M. Geers, Comput. Mater. Sci. 47 (2009) 471–481.
[50] M. Gururajan, T. Abinandanan, Acta Mater. 55 (2007) 5015–5026.
[51] D. Li, L. Chen, Acta Mater. 47 (1998) 247–257.
[52] G. Boussinot, Y. Le Bouar, A. Finel, Acta Mater. 58 (2010) 4170–4181.
[53] N. Zhou, C. Shen, M. Mills, Y. Wang, Acta Mater. 55 (2007) 5369–5381.
[54] N. Zhou, D. Lv, H. Zhang, D. McAllister, F. Zhang, M. Mills, Y. Wang, Acta Mater. 65 (2014) 270–286.
[55] L.T. Mushongera, M. Fleck, J. Kundin, Y. Wang, H. Emmerich, Acta Mater. 93 (2015) 60–72.
[56] Y.H. Wen, J.V. Lill, S.L. Chen, J.P. Simmons, Acta Mater. 58 (2010) 875–885.
[57] J. Zhang, T. Murakumo, H. Harada, Y. Koizumi, Scr. Mater. 48 (2003) 287–293.
[58] T. Link, A. Epishin, U. Brückner, P. Portella, Acta Mater. 48 (2000) 1981–1994.
[59] W. Schneider, H. Mughrabi, Creep and Fracture of Engineering Materials and Structures, 1993, pp. 209–220.
[60] R.R. Keller, H.J. Maier, H. Mughrabi, Scr. Metall. Mater. 28 (1993) 23–28.
[61] H. Gabrisch, D. Mukherji, R. Wahi, Philos. Mag. A 74 (1996) 229–249.
[62] H. Gabrisch, D. Mukherji, Acta Mater. 48 (2000) 3157–3167.
[63] G. Eggeler, A. Dlouhy, Acta Mater. 45 (1997) 4251–4262.
[64] J. Zhang, J. Wang, H. Harada, Y. Koizumi, Acta Mater. 53 (2005) 4623–4633.
[65] Y. Koizumi, T. Kobayashi, T. Yokokawa, J. Zhang, M. Osawa, H. Harada, Y. Aoki, M. Arai, Superalloys, 2004, pp. 35–43.
[66] J. Zhang, T. Murakumo, H. Harada, Y. Koizumi, Scr. Mater. 48 (2003) 287–293.
[67] T. Zhu, C.Y. Wang, Phys. Rev. B 72 (2005) 1–6.
[68] L. Carroll, Q. Feng, T. Pollock, Metall. Mater. Trans. A 39 (2008) 1290–1307.
[69] Z. Luo, Z. Wu, D.J. Miller, Mater. Sci. Eng. A 354 (2003) 358–368.
[70] R. Srinivasan, G.F. Eggeler, M.J. Mills, Acta Mater. 48 (2000) 4867–4878.
[71] A. Kostka, G. Mälzer, G. Eggeler, A. Dlouhy, S. Reese, T. Mack, J. Mater. Sci. 42 (2007) 3951–3957.
[72] J.B. le Graverend, J. Cormier, F. Gallerneau, P. Villechaise, S. Kruch, J. Mendez, Int. J. Plasticity 59 (2014) 55–83.
[73] L.A. Jácome, P. Nörtershäuser, J.K. Heyer, A. Lahni, J. Frenzel, A. Dlouhy, C. Somsen, G. Eggeler, Acta Mater. 61 (2013) 2926–2943.
[74] L.A. Jácome, P. Nörtershäuser, C. Somsen, A. Dlouhý, G. Eggeler, Acta Mater. 69 (2014) 246–264.
[75] H. Yang, M. Huang, Z. Li, Comput. Mater. Sci. 99 (2015) 348–360.
[76] Z. Zhu, H. Basoalto, N. Warnken, R. Reed, Acta Mater. 60 (2012) 4888–4900.
[77] X. Tan, J. Liu, T. Jin, Z. Hu, H. Hong, B.G. Choi, I.S. Kim, C.Y. Jo, D. Mangelinck, Mater. Sci. Eng. A 580 (2013) 21–35.
[78] B. Dyson, Mater. Sci. Technol. 25 (2009) 213–220.
[79] K. Yashiro, F. Kurose, Y. Nakashima, K. Kubo, Y. Tomita, H.M. Zbib, Int. J. Plasticity 22 (2006) 713–723.
[80] S.I. Rao, T.A. Parthasarathy, D.M. Dimiduk, P.M. Hazzledine, Philos. Mag. 84 (2004) 3195–3215.
[81] A. Vattré, B. Devincre, A. Roos, Intermetallics 17 (2009) 988–994.
[82] S.M. Hafez Haghighat, G. Eggeler, D. Raabe, Acta Mater. 61 (2013) 3709–3723.
[83] S. Gao, M. Fivel, A. Ma, A. Hartmaier, J. Mech. Phys. Solids 102 (2017) 209–223.
[84] S.S. Shishvan, R.M. McMeeking, T.M. Pollock, V.S. Deshpande, Acta Mater. 135 (2017) 188–200.
[85] S. Huang, M. Huang, Z. Li, Int. J. Plasticity 110 (2018) 1–18.
[86] P.M. Anderson, J.P. Hirth, J. Lothe, Theory of Dislocations, Cambridge University Press, Cambridge, 2017.
[87] M.F. Bartholomeusz, J.A. Wert, Metall. Mater. Trans. A 25 (1994) 2161–2171.
[88] R.D. Schmidt-Whitley, Z. Metallkd. 64 (1973) 552–560.
[89] D. Mason, D. Van Aken, Acta Metall. Mater. 43 (1995) 1201–1210.
[90] K. Hagihara, H. Araki, T. Ikenishi, T. Nakano, Acta Mater. 107 (2016) 196–212.
[91] Y. Kondo, N. Miura, T. Matsuo, Mater. Sci. Forum 539 (2007) 3100–3105.
[92] M. Pröbstle, S. Neumeier, P. Feldner, R. Rettig, H. Helmer, R. Singer, M. Göken, Mater. Sci. Eng. A 676 (2016) 411–420.
[93] P. Wollgramm, H. Buck, K. Neuking, A.B. Parsa, S. Schuwalow, J. Rogal, R. Drautz, G. Eggeler, Mater. Sci. Eng. A 628 (2015) 382–395.
[94] J.Y. Guédou, N. Tsuno, S. Takahashi, J. Choné, MATEC Web of Conf. 14 (2014) 1–4.